

## A Mechanochemical Non-hydrolytic Sol-Gel-Strategy for the Production of Mesoporous Multi-metallic Oxides

Zihao Zhang, Shize Yang, Xiaobing Hu, Haidi Xu, Honggen Peng, Miaomiao Liu, Bishnu Prasad Thapaliya, Kecheng Jie, Jiahua Zhao, Jixing Liu, Hao Chen, Yan Leng, Xiuyang Lu, Jie Fu, Pengfei Zhang, and Sheng Dai

*Chem. Mater.*, **Just Accepted Manuscript** • DOI: 10.1021/acs.chemmater.9b01244 • Publication Date (Web): 01 Jul 2019

Downloaded from <http://pubs.acs.org> on July 2, 2019

### Just Accepted

“Just Accepted” manuscripts have been peer-reviewed and accepted for publication. They are posted online prior to technical editing, formatting for publication and author proofing. The American Chemical Society provides “Just Accepted” as a service to the research community to expedite the dissemination of scientific material as soon as possible after acceptance. “Just Accepted” manuscripts appear in full in PDF format accompanied by an HTML abstract. “Just Accepted” manuscripts have been fully peer reviewed, but should not be considered the official version of record. They are citable by the Digital Object Identifier (DOI®). “Just Accepted” is an optional service offered to authors. Therefore, the “Just Accepted” Web site may not include all articles that will be published in the journal. After a manuscript is technically edited and formatted, it will be removed from the “Just Accepted” Web site and published as an ASAP article. Note that technical editing may introduce minor changes to the manuscript text and/or graphics which could affect content, and all legal disclaimers and ethical guidelines that apply to the journal pertain. ACS cannot be held responsible for errors or consequences arising from the use of information contained in these “Just Accepted” manuscripts.

# A Mechanochemical Non-hydrolytic Sol-Gel-Strategy for the Production of Mesoporous Multi-metallic Oxides

Zihao Zhang,<sup>abc</sup> Shize Yang,<sup>e</sup> Xiaobing Hu,<sup>fg</sup> Haidi Xu,<sup>c</sup> Honggen Peng,<sup>b</sup> Miaomiao Liu,<sup>c</sup>

Bishnu Prasad Thapaliya,<sup>c</sup> Kecheng Jie,<sup>c</sup> Jiahua Zhao,<sup>d</sup> Jixing Liu,<sup>c</sup> Hao Chen,<sup>a</sup> Yan Leng,<sup>c</sup>

Xiuyang Lu,<sup>a</sup> Jie Fu,<sup>a\*</sup> Pengfei Zhang<sup>d\*</sup> and Sheng Dai<sup>bc\*</sup>

<sup>a</sup> Key Laboratory of Biomass Chemical Engineering of Ministry of Education, College of Chemical and Biological Engineering, Zhejiang University, Hangzhou 310027, China

<sup>b</sup> Chemical Sciences Division, Oak Ridge National Laboratory, Oak Ridge, TN, USA

<sup>c</sup> Department of Chemistry, The University of Tennessee, Knoxville, TN, USA

<sup>d</sup> School of Chemistry and Chemical Engineering, Shanghai Jiao Tong University, Shanghai 200240, China

<sup>e</sup> Center for Functional Nanomaterials, Brookhaven National Laboratory, Upton, NY11973, USA

<sup>f</sup> Department of Materials Science and Engineering, Northwestern University, Evanston, IL 60208, USA

<sup>g</sup> The NUANCE Center, Northwestern University, Evanston, IL 60208, USA

\*Corresponding author: Jie Fu, E-mail: [jjefu@zju.edu.cn](mailto:jjefu@zju.edu.cn)

Pengfei Zhang, E-mail: [chemistryzpf@sjtu.edu.cn](mailto:chemistryzpf@sjtu.edu.cn)

Sheng Dai, E-mail: [dais@ornl.gov](mailto:dais@ornl.gov)

**Abstract:** Mesoporous metal oxides with wide pore size, high surface area and uniform

porous structures have demonstrated excellent advantages in various fields. However, the state-of-art synthesis approaches are dominated by wet chemistry, accompanied by use of excessive solvent, and the requirement of time-consuming drying process. Herein, we report a mechanochemical solid-state route to synthesize mesoporous  $\text{Al}_2\text{O}_3$  (meso- $\text{Al}_2\text{O}_3$ ) via aluminum isopropoxide-copolymers assembly. The obtained meso- $\text{Al}_2\text{O}_3$  shows a record high surface area ( $\sim 644 \text{ m}^2 \text{ g}^{-1}$ ) and narrow pore size distribution (centered at  $\sim 5 \text{ nm}$ ). Moreover, a mechanochemical nonhydrolytic sol-gel strategy is introduced to fabricate mesoporous transition metal (Cu, Co, Mn, Fe, Mg, Ni)-aluminium binary oxide by using anhydrous metal chlorides and aluminum isopropoxide interplay. More importantly, four or five metals-aluminum oxide complexes with abundant mesopores and single cubic crystalline phase known as high-entropy ceramics are produced. To the best of our knowledge, mesoporous high-entropy metal oxides have not been prepared before, because the high crystallization temperature would make mesopores collapse. Additionally, this high-entropy property endows  $(\text{CuNiFeCoMg})\text{O}_x\text{-Al}_2\text{O}_3$  with superior  $\text{SO}_2$ -resisting performance (1000 ppm  $\text{SO}_2$  in  $\text{N}_2$  at  $280 \text{ }^\circ\text{C}$ ) in the catalytic oxidation of CO compared to single  $\text{CuO-Al}_2\text{O}_3$ .

## 1. Introduction

Mesoporous metal oxides with wide pore size, high surface area, uniform pore size distribution as well as a variety of structures and compositions endow them particularly

1  
2  
3  
4  
5 attractive for applications in catalysis, adsorption, battery technology, sensing, and so on.<sup>[1-</sup>  
6  
7  
8 <sup>6]</sup> Template-assisted processes via either soft- or hard templates were usually used for the  
9  
10 synthesis of mesoporous metal oxides.<sup>[7-12]</sup> In general, the hard-templating technique relied  
11  
12 on mesoporous silica or carbon aerogel as the hard templates, which inevitably required  
13  
14 additional steps and costs.<sup>[9,13-21]</sup> In comparison, organic-inorganic assembly routes, using  
15  
16 block co-polymers or surfactants as soft templates have been developed as a more  
17  
18 straightforward method.<sup>[22-26]</sup> It is undeniable that the solvent evaporation-induced self-  
19  
20 assembly method has been successfully applied into the synthesis of many mesoporous metal  
21  
22 oxides.<sup>[27-29]</sup> However, several issues seem left in this wet soft-templating process, including:  
23  
24  
25  
26  
27  
28  
29 1) Excessive organic solvents are used; 2) It requires the metal precursors that have to be  
30  
31 dissolved in the solvents, which limits the applications of many insoluble metal  
32  
33 precursors;<sup>[3,30]</sup> 3) The slow solvent evaporation is a time-consuming step.<sup>[31]</sup>  
34  
35  
36  
37

38 To resolve these disadvantages, solid-state synthesis, an old method in material  
39  
40 processing, has been revisited.<sup>[32-35]</sup> Several porous materials, such as zeolite, metal-organic  
41  
42 frameworks, covalent-organic frameworks, ordered mesoporous polymers and mesoporous  
43  
44 carbons have been already synthesized via mechanochemical processes.<sup>[36-38]</sup> Although, a  
45  
46 solvent-free assembly method has also been introduced for the construction of mesoporous  
47  
48 metal oxide (TiO<sub>2</sub>), this route needs HCl as the solvent and aged at 140 °C for 24 h before  
49  
50 calcination, making it not a “true” solvent-free system.<sup>[37]</sup> As a result, the synthesis of  
51  
52  
53  
54  
55  
56  
57  
58  
59  
60

1  
2  
3  
4  
5 mesoporous metal oxides via mechanochemical solid-state method, especially for metal  
6  
7  
8 oxides hybrids, is highly welcome. Moreover, alumina has been widely used as an important  
9  
10 carrier in catalysis, and alumina-based mixed mesoporous metal oxides also display  
11  
12 extensive application prospect.<sup>[39-43]</sup> Therefore, the one-pot preparation of mesoporous  
13  
14 alumina-supported metal oxides via mechanochemical solid-state method seems like a more  
15  
16 efficient and straightforward pathway toward industrial catalysis.  
17  
18  
19  
20

21       Herein, we demonstrate the facile, rapid and solid-state synthesis of mesoporous  
22  
23 aluminum oxide (meso- $\text{Al}_2\text{O}_3$ ) by a mechanochemical assembly between aluminum  
24  
25 isopropoxide and commercial polymers (e.g., PEO-PPO-PEO, P123; polyethylene glycol,  
26  
27 PEO, PEG). Moreover, binary Al-based oxides (Cu, Co, Mn et al.) with abundant mesopores  
28  
29 can be easily constructed by mechanochemical nonhydrolytic sol-gel process (NHSG, metal  
30  
31 chlorides and aluminum isopropoxide interplay).<sup>[44-46]</sup> More interestingly, four or five  
32  
33 transition metal species-aluminum oxide hybrids—the so-called high-entropy oxides—with  
34  
35 single cubic crystalline phase and rich mesoporous structure were synthesized via this  
36  
37 mechanochemical NHSG method. To our surprise, the high-entropy feature endows  
38  
39  $(\text{CuNiFeCoMg})\text{O}_x\text{-Al}_2\text{O}_3$  with superior  $\text{SO}_2$ -resisting performance (1000 ppm  $\text{SO}_2$  in  $\text{N}_2$  at  
40  
41 280 °C) in the catalytic oxidation of CO compared to  $\text{CuO-Al}_2\text{O}_3$ .  
42  
43  
44  
45  
46  
47  
48  
49  
50  
51  
52  
53  
54  
55  
56  
57  
58  
59  
60

## 2. Experimental Section

### 2.1 Catalyst synthesis

*meso-Al<sub>2</sub>O<sub>3</sub>*: 1 g metal precursor (aluminum isopropoxide) and 0.2 g ~ 0.4 g soft templates (Pluronic P123: 5800g mol<sup>-1</sup>; PEG: 4000 g mol<sup>-1</sup>, Pluronic F127 (F127) and cetyltrimethylammonium bromide (CTAB)) were added in a 9.5 mL screw-capped iron reactor with two big (diameter: 1.2 cm) and three small (diameter: 0.5 cm) iron steel ball bearings. The sealed reactor was placed in a high-speed vibrating ball miller (Retsch MM400), and the mixtures were ball milled for 60 min at a vibrational frequency of 30 Hz. The resulting samples were washed using ethanol and dried at 40 °C under vacuum conditions, followed by calcinating at 400 °C with the heating rate of 2 °C min<sup>-1</sup>.

*mesoporous binary metal oxides (Cu, Co, and Mn et al.)*: Aluminum isopropoxide (2.67 mmol) and a transition metal chloride (4 mmol) as well as 0.4 g PEG were added in in a 9.5 mL screw-capped iron reactor with two big (diameter: 1.2 cm) and three small (diameter: 0.5 cm) iron steel ball bearings. After ball milling for 60 min, the post-treatment procedure is same with the synthesis of *meso-Al<sub>2</sub>O<sub>3</sub>*. All catalysts were washed using water for three times before use.

*(CuNiFeCo)<sub>x</sub>-Al<sub>2</sub>O<sub>3</sub>*: Aluminum isopropoxide (2.67 mmol), cooper chloride (1 mmol), nickel chloride (1 mmol), cobalt chloride (1 mmol) and ferrous chloride (1 mmol), as well as

1  
2  
3  
4  
5 0.4 g PEG are added in in a 9.5 mL screw-capped iron reactor with two big (diameter: 1.2  
6  
7 cm) and three small (diameter: 0.5 cm) iron steel ball bearings. After ball milling for 60 min,  
8  
9 the post-treatment procedure is same with the synthesis of meso- $\text{Al}_2\text{O}_3$ .  
10  
11

12  
13  $(\text{CuNiFeCoMg})_x\text{-Al}_2\text{O}_3$ : Aluminum isopropoxide (3.33 mmol), cooper chloride (1  
14  
15 mmol), nickel chloride (1 mmol), cobalt chloride (1 mmol), ferrous chloride (1 mmol) and  
16  
17 Magnesium chloride (1 mmol), as well as 0.4 g PEG are added in in a 9.5 mL screw-capped  
18  
19 iron reactor with two big (diameter: 1.2 cm) and three small (diameter: 0.5 cm) iron steel ball  
20  
21 bearings. After ball milling for 60 min, the post-treatment procedure is same with the  
22  
23 synthesis of meso- $\text{Al}_2\text{O}_3$ .  
24  
25  
26  
27  
28  
29

## 30 **2.2 Characterizations**

31  
32  
33

34 X-rays diffraction (XRD) was collected on a PANalytical Empyrean diffractometer  
35  
36 operated at 45 kV and 40 mA (scanning step:  $0.02^\circ$  per step).  $\text{N}_2$  adsorption-desorption  
37  
38 isotherms were analyzed on a TriStar 3000 volumetric adsorption analyzer manufactured and  
39  
40 by Micromeritics Instrument Corp. A classical Barrett–Joyner–Halenda (BJH) method was  
41  
42 employed to determine the pore size distribution by using adsorption branch of isotherms.  
43  
44 Prior to analysis, all samples were activated at  $160^\circ\text{C}$  for 8 h. Scanning electron microscopy  
45  
46 (SEM) with energy-dispersive X-ray spectroscopy (EDS) mapping results was recorded  
47  
48 using a Zeiss EVO-MA15 scanning electron microscope with a Bruker XFlash 6130 detector.  
49  
50  
51  
52  
53  
54  
55  
56  
57  
58  
59  
60

1  
2  
3  
4  
5 Scanning electron microscopy (SEM) images was recorded using a Zeiss AURIGA.  
6  
7  
8 Scanning transmission electron microscopy (STEM) was performed on a Nion microscope  
9  
10 operated at 200 kV and ARM 200CF equipped with a probe corrector. The images are  
11  
12 recorded using high angle annular dark field (HAADF) and bright field (BF) imaging. X-ray  
13  
14 photoelectron spectroscopy (XPS) was performed by AXIS Ultra DLD spectrometer (Kratos,  
15  
16 Japan). The obtained data was calibrated by C 1s standard peak and analyzed by Casa XPS  
17  
18 software. Temperature programmed desorption (TPD) of CO was recorded using FineSorb-  
19  
20 3010 from Zhejiang FINETEC INSTRUMENTS co., LTD with a thermal conductivity  
21  
22 detector (TCD). Prior to characterization, fresh and spent catalysts were preheated at 120 °C  
23  
24 under argon atmosphere. Elemental analysis of the samples was done by inductively coupled-  
25  
26 plasma atomic emission spectroscopy (ICP-AES) using the Optima 2100 DV spectrometer  
27  
28 (PerkinElmer Corporation). The actual metal ratios are summarized in Table S1. Fourier  
29  
30 Transform infrared spectroscopy (FTIR) spectra was collected on a Bio-Rad FTIR  
31  
32 spectrometer (Excalibur series).  
33  
34  
35  
36  
37  
38  
39  
40  
41  
42  
43

### 44 **2.3 Experimental procedures**

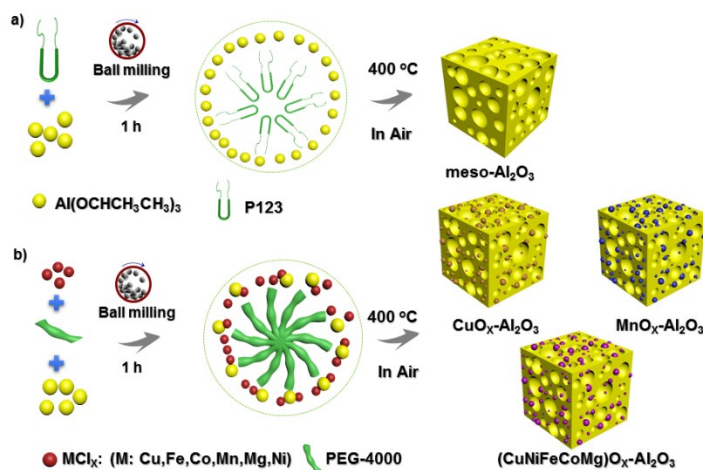
45  
46  
47 CO oxidation experiments were carried out in a fixed bed reactor (straight quartz tube  
48  
49 with 4 mm inner diameter) at atmospheric pressure. For the measurement of CO light-off  
50  
51 curves showing CO conversion as a function of reaction temperature, 20 mg of catalyst  
52  
53  
54  
55  
56  
57  
58  
59  
60

1  
2  
3  
4  
5 supported by quartz wool was loaded in the reactor. The feed gas of 1% CO balanced with  
6  
7  
8 dry air (< 4 ppm water) passed through the catalyst bed at a flow rate of 10 mL/min  
9  
10  
11 corresponding to a gas hourly space velocity (GHSV) of 30,000 mL/(h g cat). The  
12  
13 concentrations of CO and CO<sub>2</sub> in the reactor were analyzed by a Buck Scientific 910 gas  
14  
15 chromatograph equipped with a dual molecular sieve/porous polymer column (Alltech CTR1)  
16  
17 and a thermal conductivity detector. CO conversion is calculated as the peak areas of CO of  
18  
19 consumption divided by that of CO before the reaction.  
20  
21  
22  
23

### 24 **3. Results and discussion**

25  
26  
27 **Scheme 1** summarizes a mechanochemical route for the synthesis of meso-Al<sub>2</sub>O<sub>3</sub> and  
28  
29 related metal oxide hybrids using aluminum isopropoxide and anhydrous metal chlorides as  
30  
31 the precursors, and P123 or PEG as the soft template. An efficient assembly between  
32  
33 aluminum isopropoxide and P123 micelles is realized by mechanically grinding the mixture  
34  
35 in a vibrating ball miller for 60 min (much shorter than the traditional solvent evaporation  
36  
37 induced assembly process, 1 ~ 3 days in most cases).<sup>[23,47]</sup> It has been reported that the  
38  
39 condensation between chloride and alkoxide by mixing the chloride precursors (MCl<sub>x</sub>) and  
40  
41 oxygen donor (Al(OR)<sub>3</sub>) to produce the xerogels is considered as NHSG process<sup>[48]</sup>. The  
42  
43 resulting xerogels is then washed and dried under vacuum and finally calcined in air to  
44  
45 achieve the corresponding metal oxides. In this work, the mechanochemical NHSG process  
46  
47  
48  
49  
50  
51  
52  
53  
54 between metal chlorides and aluminum isopropoxide in the solid-state via complex  
55  
56  
57  
58  
59  
60

mechanism is restricted to the periphery of micelles. The obtained xerogels is performed by XRD (Figure S1) and then calcinated at 400 °C in air to remove template. By combining with aluminum isopropoxide-copolymers crosslinking and NHSG process in one-step, the mixed oxides with uniform mesopores can be prepared.



**Scheme 1.** The schematic diagram for the synthesis of meso- $\text{Al}_2\text{O}_3$ , mesoporous mixed metal oxides using mechanochemical NHSG method.

The textural properties of the as-synthesized  $\text{Al}_2\text{O}_3$  without and with different surfactants are summarized (**Table 1**) by  $\text{N}_2$  adsorption-desorption isotherms at 77 K in Figure S2. The blank  $\text{Al}_2\text{O}_3$  sample without templates offers a low surface area ( $246 \text{ m}^2 \text{ g}^{-1}$ ) with a broad pore size distribution in Figure S2a,c. In comparison, a meso- $\text{Al}_2\text{O}_3$  sample with 0.2g P123 as the template gives a type-IV isotherm with a H3-type hysteresis loop, resulting in both high surface area ( $415 \text{ m}^2 \text{ g}^{-1}$ ) and narrow pore size distribution centered at  $\sim 3 \text{ nm}$  (Figure S2). For meso- $\text{Al}_2\text{O}_3$ , a higher calcination temperature at 800 °C will lead to the collapse of a portion of mesopores, as seen in Figure S3. Additionally, PEG, F127 and CTAB

1  
2  
3  
4  
5 as templates also contribute to the formation of mesopores smaller than 10 nm (**Table 1**). The  
6  
7 weight ratio of P123/Al precursor exhibits significant influence for the formation of  
8  
9 mesopores. The N<sub>2</sub> adsorption-desorption isotherms and pore size distribution results of  
10  
11 meso-Al<sub>2</sub>O<sub>3</sub> synthesized with 0.4 g P123 displays a higher surface area of 644 m<sup>2</sup> g<sup>-1</sup> and  
12  
13 narrower pore size distribution of ~5 nm (**Figure 1a,b**). It is noteworthy that the difference  
14  
15 between average pore size from **Table 1** and pore size distribution from **Figure 1** should be  
16  
17 ascribed to the limitation and accuracy of BJH model used. The transmission electron  
18  
19 microscopy (TEM) and scanning transmission electron microscopy (STEM) image of meso-  
20  
21 Al<sub>2</sub>O<sub>3</sub> with 0.4g P123 as the template also reveal the existence of a sponge-like  
22  
23 nanoarchitecture with a large number of apparent mesopores (**Figure 2a,b**). A portion of  
24  
25 mesopores is marked by yellow circles from STEM-EDS image in Figure S4. The wide-angle  
26  
27 X-ray diffraction (XRD) result of meso-Al<sub>2</sub>O<sub>3</sub> calcined at 400 °C with different templates  
28  
29 shows an amorphous structure (**Figure 3a, S5**).

30  
31  
32  
33  
34  
35  
36  
37  
38  
39  
40 **Table 1.** Summary of pore parameter for different metal oxides calculated using N<sub>2</sub>  
41  
42 adsorption-desorption isotherms at 77 K.

Samples	S <sub>BET</sub> (m <sup>2</sup> g <sup>-1</sup> )	Pore volume (cm <sup>3</sup> g <sup>-1</sup> )	Average pore size (nm)
Al <sub>2</sub> O <sub>3</sub>	246	0.32	~
meso-Al <sub>2</sub> O <sub>3</sub> (0.4 g P123)	644	0.75	4.2
meso-Al <sub>2</sub> O <sub>3</sub> (0.2 g PEG)	257	0.16	2.3

meso-Al <sub>2</sub> O <sub>3</sub> (0.2 g CTAB)	380	0.26	~
meso-Al <sub>2</sub> O <sub>3</sub> (0.2 g F127)	329	0.24	~
meso-Al <sub>2</sub> O <sub>3</sub> (0.2 g P123)	415	0.34	2.6
CuO-Al <sub>2</sub> O <sub>3</sub>	115	0.11	2.8
Mn <sub>3</sub> O <sub>4</sub> -Al <sub>2</sub> O <sub>3</sub>	143	0.27	4.9
Co <sub>3</sub> O <sub>4</sub> -Al <sub>2</sub> O <sub>3</sub>	133	0.14	7.2
Fe <sub>2</sub> O <sub>3</sub> -Al <sub>2</sub> O <sub>3</sub>	178	0.24	5.8
NiO-Al <sub>2</sub> O <sub>3</sub>	168	0.15	3.3
MgO-Al <sub>2</sub> O <sub>3</sub>	176	0.18	6.3
(CuNiFeCo) <sub>x</sub> -Al <sub>2</sub> O <sub>3</sub>	129	0.13	3.9
(CuNiFeCoMg) <sub>x</sub> -Al <sub>2</sub> O <sub>3</sub>	198	0.24	4.8

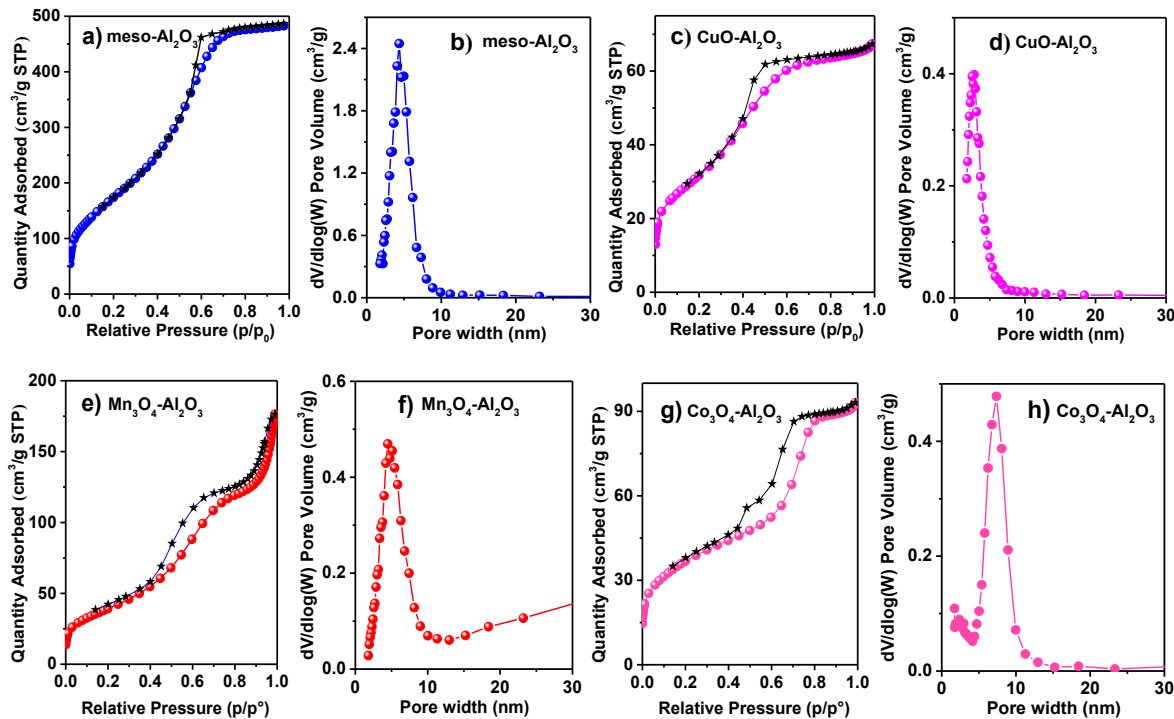
<sup>a</sup>Specific surface area calculated using the BET equation.

<sup>b</sup>Single point adsorption total pore volume of pores.

<sup>c</sup>Average pore diameter from the distribution maxima by resolving adsorption branch with BJH model.

Compared with monometallic oxide, binary metal oxides tend to possess wider applications in catalysis. The traditional NHSG method for the production of metal oxides often takes place in organic solvents and the corresponding pore size distribution is much wide.<sup>[46,48]</sup> By the mechanochemical NHSG route in the solid-state, mesoporous binary metal oxides (CuO-Al<sub>2</sub>O<sub>3</sub>, Mn<sub>3</sub>O<sub>4</sub>-Al<sub>2</sub>O<sub>3</sub> and Co<sub>3</sub>O<sub>4</sub>-Al<sub>2</sub>O<sub>3</sub>) with uniform pore size distribution could be successfully synthesized with optimized PEG as the optimized template (**Figure 1c-h**; Figure S6). In comparison to P123 and F127, PEG is a more safe, cheap and renewable

1  
2  
3  
4  
5 material. However, PEG has been used as soft templates with only limited success in  
6  
7  
8 directing mesopores until now. XRD results reveal the clear crystalline structures of CuO  
9  
10 [JCPDS 44-0706],  $\text{Mn}_3\text{O}_4$  [JCPDS 18-0803] and  $\text{Co}_3\text{O}_4$  [JCPDS 43-1003] in  $\text{CuO-Al}_2\text{O}_3$ ,  
11  
12  $\text{Mn}_3\text{O}_4\text{-Al}_2\text{O}_3$  and  $\text{Co}_3\text{O}_4\text{-Al}_2\text{O}_3$  samples respectively (**Figure 3a**), and the corresponding  
13  
14 crystalline size calculated by Scherrer equation are 15.9, 13.4 and 11.8 nm respectively.  
15  
16  
17 Additionally, no diffraction peaks associated with  $\text{Al}_2\text{O}_3$  can be found in three binary metal  
18  
19 oxides. Moreover, the diffraction peaks corresponding to NiO, MgO and  $\text{Fe}_2\text{O}_3$  crystalline  
20  
21 phase respectively were discovered in the  $\text{NiO-Al}_2\text{O}_3$ ,  $\text{MgO-Al}_2\text{O}_3$  and  $\text{Fe}_2\text{O}_3\text{-Al}_2\text{O}_3$  samples  
22  
23  
24 respectively, as shown in XRD results (Figure S7).  
25  
26  
27  
28  
29



1  
2  
3  
4  
5 **Figure 1.** N<sub>2</sub> adsorption-desorption isotherms (a,c,e,g) and the corresponding pore size  
6 distribution (b,d,f,h) of meso-Al<sub>2</sub>O<sub>3</sub>, CuO-Al<sub>2</sub>O<sub>3</sub>, Mn<sub>3</sub>O<sub>4</sub>-Al<sub>2</sub>O<sub>3</sub> and Co<sub>3</sub>O<sub>4</sub>-Al<sub>2</sub>O<sub>3</sub>  
7 synthesized using mechanochemical NHSG method.  
8  
9

10  
11  
12  
13  
14 The surface area and pore structure of CuO-Al<sub>2</sub>O<sub>3</sub>, Mn<sub>3</sub>O<sub>4</sub>-Al<sub>2</sub>O<sub>3</sub> and Co<sub>3</sub>O<sub>4</sub>-Al<sub>2</sub>O<sub>3</sub>  
15 were examined with N<sub>2</sub> adsorption-desorption isotherm measurements (**Figure 1c,e,g**). All  
16 samples show representative type-IV curves with clear capillary condensation steps between  
17 the relative pressure (P/P<sub>0</sub>) of 0.4–0.8, underscoring the presence of rich mesopores. The  
18 specific surface areas of CuO-Al<sub>2</sub>O<sub>3</sub>, Mn<sub>3</sub>O<sub>4</sub>-Al<sub>2</sub>O<sub>3</sub> and Co<sub>3</sub>O<sub>4</sub>-Al<sub>2</sub>O<sub>3</sub> are 115, 144 and 133  
19 m<sup>2</sup> g<sup>-1</sup>, respectively (**Table 1**). More importantly, the pore size distributions by resolving the  
20 adsorption branch of N<sub>2</sub> isotherms with Barrett-Joyner-Halenda (BJH) method centred at 4,  
21 6 and 7 nm for CuO-Al<sub>2</sub>O<sub>3</sub>, Mn<sub>3</sub>O<sub>4</sub>-Al<sub>2</sub>O<sub>3</sub> and Co<sub>3</sub>O<sub>4</sub>-Al<sub>2</sub>O<sub>3</sub> respectively (**Figure 1d,f,h**).<sup>149</sup>  
22  
23 Moreover, N<sub>2</sub> adsorption and pore size distribution results of NiO-Al<sub>2</sub>O<sub>3</sub>, MgO-Al<sub>2</sub>O<sub>3</sub> and  
24 Fe<sub>2</sub>O<sub>3</sub>-Al<sub>2</sub>O<sub>3</sub> samples also reveal the existence of abundant mesoporous structure (**Table 1**;  
25  
26  
27  
28  
29  
30  
31  
32  
33  
34  
35  
36  
37  
38  
39  
40  
41  
42  
43  
44  
45  
46  
47  
48  
49  
50  
51  
52  
53  
54  
55  
56  
57  
58  
59  
60  
Figure S8). These obtained abundant and uniform mesopores in binary metal oxides should  
be ascribed to solid-state self-assembly behavior of PEG micelles and different metal ions,  
confining NHSG process within the periphery of micelles. The results indicate that the  
mechanochemical NHSG route has the traits of universality for the preparation of a variety  
of binary metal oxides with uniform mesopore distributions. Additionally, the obtained  
surface area for both meso-Al<sub>2</sub>O<sub>3</sub> and binary metal oxides are comparable to the previously

1  
2  
3  
4  
5 reported mesoporous alumina and metal containing mesoporous alumina synthesized by  
6  
7 conventional wet chemistry<sup>[24,50]</sup>.  
8  
9

10  $\text{Mn}_3\text{O}_4\text{-Al}_2\text{O}_3$  is then chosen as a representative to investigate the pore structure of  
11  
12 binary metal oxides in a more tangible manner. Wormhole architectures with rich mesopores  
13  
14 side by side are observed throughout the material backbone in the range of several hundred  
15  
16 nanometers (**Figure 2c,d**). Furthermore, energy-dispersive X-ray spectroscopy (EDS)  
17  
18 mapping results of representative binary  $\text{Mn}_3\text{O}_4\text{-Al}_2\text{O}_3$  sample (**Figure 2e-g**; Figure S9) show  
19  
20 the well distribution of Mn, Al and O, suggesting that the mesoporous structure is fabricated  
21  
22 by the uniform mixture of  $\text{Mn}_3\text{O}_4$  and  $\text{Al}_2\text{O}_3$ . Additionally, TEM and EDS-mapping results  
23  
24 for  $\text{CuO-Al}_2\text{O}_3$  and  $\text{Co}_3\text{O}_4\text{-Al}_2\text{O}_3$  samples in Figure S10,11 also display existence of  
25  
26 mesopores and unifrom mixture of CuO ( $\text{Co}_3\text{O}_4$ ) and  $\text{Al}_2\text{O}_3$ .  
27  
28  
29  
30  
31  
32  
33  
34  
35  
36  
37  
38  
39  
40  
41  
42  
43  
44  
45  
46  
47  
48  
49  
50  
51  
52  
53  
54  
55  
56  
57  
58  
59  
60

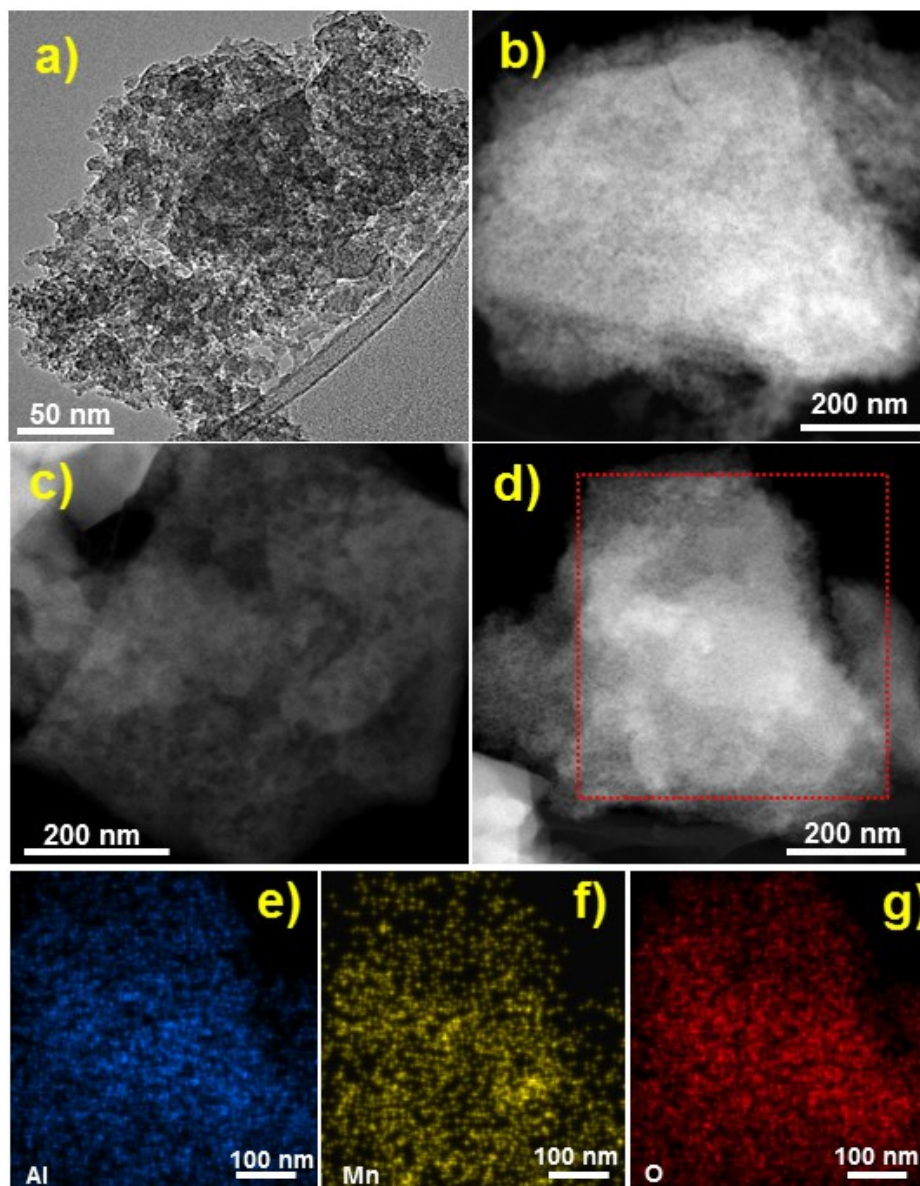


**Figure 2.** TEM a) and STEM-HAADF b) images of meso- $\text{Al}_2\text{O}_3$ ; STEM-HAADF images (c,d) of  $\text{Mn}_3\text{O}_4\text{-Al}_2\text{O}_3$  and the corresponding element mapping signals e) Al, f) Mn and g) O.

Interestingly, the XRD result of  $(\text{CuNiFeCo})\text{O}_x\text{-Al}_2\text{O}_3$  sample synthesized by the same method does not show the characteristic diffraction peaks of  $\text{CuO}$ ,  $\text{Fe}_2\text{O}_3$  or  $\text{Co}_3\text{O}_4$

1  
2  
3  
4  
5 (Figure S12). The XRD pattern of  $(\text{CuNiFeCo})\text{O}_x\text{-Al}_2\text{O}_3$  reveals its crystalline structure,  
6  
7  
8 which is close to 37.2 (111), 43.3 (012), 62.8 (110) and 75.4 (113) reflections of cubic NiO  
9  
10 (JCPDS 65-2901). Above results suggest that Cu, Fe and Co may be incorporated into the  
11  
12 sublattice of NiO to form a solid solution. STEM-HAADF images of  $(\text{CuNiFeCo})\text{O}_x\text{-Al}_2\text{O}_3$   
13  
14 sample reveal the aggregations of hybrid crystallites with a high degree of interstitial porosity  
15  
16  
17  
18 (**Figure 4a,b**). EDS-mapping results show the highly uniform distribution of four metal  
19  
20 species (Cu, Ni, Fe and Co), further suggesting the existence of  $(\text{CuNiFeCo})\text{O}_x$  solid solution  
21  
22 (Figure S13). The pore nature of  $(\text{CuNiFeCo})\text{O}_x\text{-Al}_2\text{O}_3$  sample was then evaluated via  $\text{N}_2$   
23  
24 adsorption-desorption measurement at 77 K. A type-IV isotherm with an  $\text{H}_3$  type hysteresis  
25  
26 loop between the relative  $P/P_0$  of 0.4 to 0.7 can be observed, leading to a surface area of 129  
27  
28  
29  
30  $\text{m}^2 \text{g}^{-1}$  (**Table 1**) with narrow pore size distribution ( $\sim 4 \text{ nm}$ ) (**Figure 5a,b**). The molar ratio  
31  
32 of Al:(CuNiFeCo) obtained from ICP-AES result is 1.9, similar with 1.5 determined from  
33  
34  
35  
36  
37  
38 EDS result in Figure S13.  
39  
40  
41  
42  
43  
44  
45  
46  
47  
48  
49  
50  
51  
52  
53  
54  
55  
56  
57  
58  
59  
60

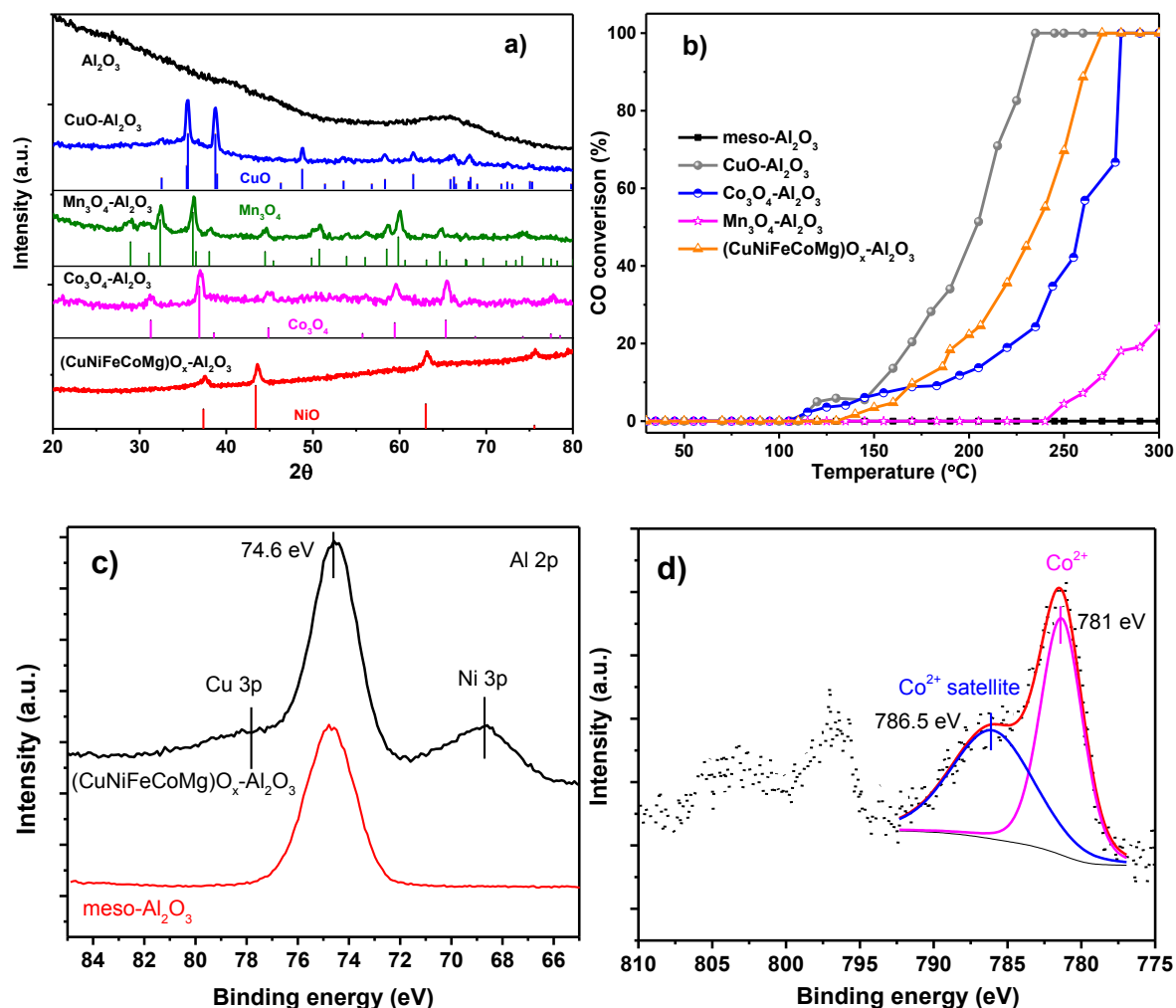


**Figure 3.** XRD results of a)  $\text{meso-Al}_2\text{O}_3$ , binary metal oxides and  $(\text{CuNiFeCoMg})\text{O}_x\text{-Al}_2\text{O}_3$ ; b) CO oxidation activity over different catalysts; Normalized XPS spectra of c) Al 2p and d) Co 2p transitions for  $\text{meso-Al}_2\text{O}_3$  (peak intensity for Al 2p is reduced) and  $(\text{CuNiFeCoMg})\text{O}_x\text{-Al}_2\text{O}_3$  samples.

Crystalline high-entropy metal oxides (normally containing five or more metal species), as a new class of material, have attracted great interest because of their unique structure and potential applications.<sup>[51,52]</sup> To date, the state-of-art high-entropy metal oxides only possess very limited surface area (e.g.,  $<30 \text{ m}^2 \text{ g}^{-1}$ )<sup>[53,54]</sup>, because their porous structures

1  
2  
3  
4  
5 would collapse during the removal of templates and the crystallization process, which limits  
6  
7 their performance in catalysis. To synthesize mesoporous high entropy metal-Al mixed  
8  
9 oxides, Mg was chosen as the fifth metal element for the preparation of  $(\text{CuNiFeCoMg})\text{O}_x$ -  
10  
11  $\text{Al}_2\text{O}_3$ . The basis for the choice of these metals is their similar atomic radius. The  
12  
13 corresponding XRD patterns are displayed (**Figure 3a**). It is reassuring that when Mg is used  
14  
15 as the fifth metal, the diffraction peaks become similar with the shift of diffraction peaks of  
16  
17 cubic crystalline NiO. The diffraction peaks belonging to CuO,  $\text{Fe}_2\text{O}_3$ ,  $\text{Co}_3\text{O}_4$  and  $\text{Mn}_3\text{O}_4$  in  
18  
19 binary metal-Al oxides disappeared accidentally, suggesting the formation of single high-  
20  
21 entropy phase). The crystalline size of high-entropy phase is approximately 11.6 nm  
22  
23 determined by Scherrer equation. Moreover, SEM-EDS results reveal that five elements (Cu,  
24  
25 Ni, Fe, Co and Mg) signal are simultaneous discovered in selected regions (**Figure 4e-l**). The  
26  
27 obtained results suggested that the high-entropy metal oxides  $(\text{CuNiFeCoMg})\text{O}_x$  should be  
28  
29 formed and mixed uniformly with  $\text{Al}_2\text{O}_3$  to form a mesoporous complex. We deduced that  
30  
31 the mechanochemical process together with calcination step in are the major reason for the  
32  
33 formation of solid solution.  
34  
35  
36  
37  
38  
39  
40  
41  
42  
43  
44

45  
46 The metal valence is illustrated by X-ray photoelectron spectroscopy (XPS) analysis,  
47  
48 and the results are shown in **Figure 3c,d** and Figure S14. The Al 2p XPS spectra in **Figure**  
49  
50 **3c** show the primary peak located at 74.6 eV for both meso- $\text{Al}_2\text{O}_3$  and  $(\text{CuNiFeCoMg})\text{O}_x$ -  
51  
52  $\text{Al}_2\text{O}_3$  samples, suggesting the existence of Al-O bonds in  $\text{Al}^{3+}$  (often known as  $\text{Al}_2\text{O}_3$ )  
53  
54  
55  
56  
57  
58  
59  
60

1  
2  
3  
4  
5 species). The Cu 2p spectrum in Figure S14a can be fitted into four peaks, corresponding to  
6  
7 Cu 2p<sub>3/2</sub> (933.0 eV) and Cu 2p<sub>1/2</sub> (953.0 eV) and their satellite peaks. These characteristics  
8  
9 match well with standard peaks of CuO. The similar results in Ni 2p spectrum can identify  
10  
11 the possible existence of NiO (Figure S14b)<sup>[55]</sup>. The main peak from Mg 2p spectrum in  
12  
13 Figure S14c is located around 50 eV, but valence state of Mg is difficult to be determined  
14  
15 due to the close peak position of different state (Mg<sup>0</sup> and Mg<sup>2+</sup>). However, Mg should exist  
16  
17 in MgO form considering that the synthesis process is difficult to generate Mg<sup>0</sup>. For Co 2p  
18  
19 spectrum in **Figure 3d**, the peaks at 781 eV together with strong satellite at 786.5 eV indicate  
20  
21 the existence of Co<sup>2+</sup>, since the signature of Co<sup>3+</sup> have no satellite peak<sup>[56]</sup>. The Fe 2p  
22  
23 spectrum in Figure S14d suggests the co-existence of Fe<sup>2+</sup> and Fe<sup>3+</sup>.  
24  
25  
26  
27  
28  
29  
30  
31

32  
33 STEM-HAADF images of (CuNiFeCoMg)O<sub>x</sub>-Al<sub>2</sub>O<sub>3</sub> sample suggest the existence of  
34  
35 rich mesoporosity marked with small yellow circles (**Figure 4c-d**), which is also revealed by  
36  
37 SEM images in Figure S15. The pore nature of (CuNiFeCoMg)O<sub>x</sub>-Al<sub>2</sub>O<sub>3</sub> sample was then  
38  
39 evaluated by N<sub>2</sub> adsorption-desorption measurement at 77 K. A type-IV isotherm with steep  
40  
41 adsorption peaks between the relative pressure (P/P<sub>0</sub>) of 0.2–0.8, revealing the abundant  
42  
43 mesoporous structure (**Figure 5c,d**). It offered a surface area up to 198 m<sup>2</sup> g<sup>-1</sup>, and the relative  
44  
45 lower surface area compared to meso-Al<sub>2</sub>O<sub>3</sub> should be attributed to the blockage and collapse  
46  
47 of pore channels during the crystallization process of high-entropy metal oxides. The molar  
48  
49 ratio of Al:(CuNiFeCoMg) obtained from ICP-AES result is 1.3.  
50  
51  
52  
53  
54  
55  
56  
57  
58  
59  
60

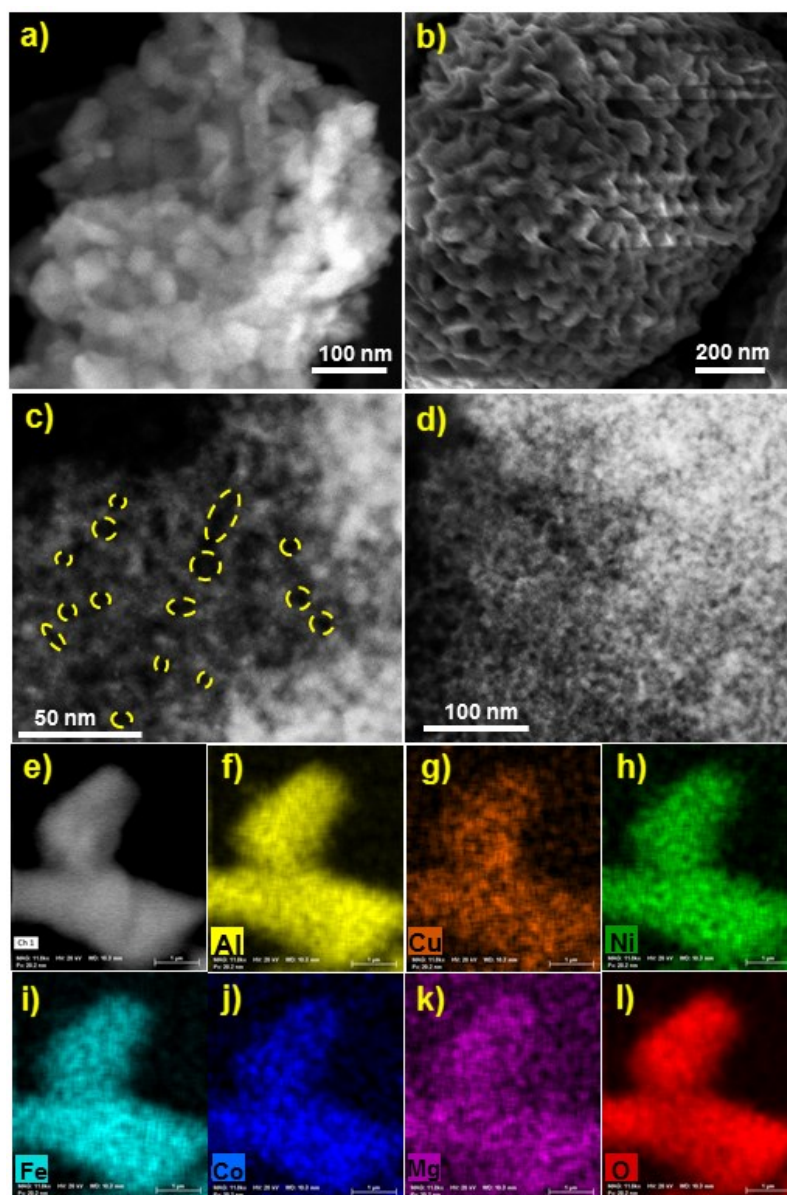


**Figure 4.** STEM (a) and SEM (b) images of (CuNiFeCo)O<sub>x</sub>-Al<sub>2</sub>O<sub>3</sub>; STEM (c,d) images of (CuNiFeCoMg)O<sub>x</sub>-Al<sub>2</sub>O<sub>3</sub>; SEM-EDS image (e) of (CuNiFeCoMg)O<sub>x</sub>-Al<sub>2</sub>O<sub>3</sub> and the corresponding element mapping signals f) Al, g) Cu, h) Ni, i) Fe, j) Co, k) Mg, l) O.

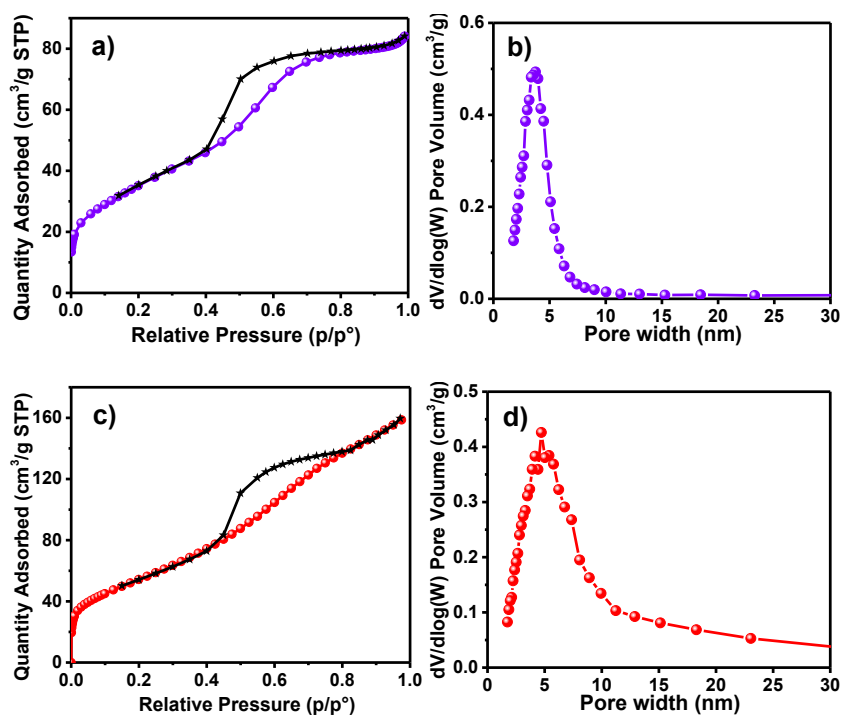


**Figure 5.** N<sub>2</sub> adsorption-desorption isotherms and the corresponding pore size distribution of (CuNiFeCo)O<sub>x</sub>-Al<sub>2</sub>O<sub>3</sub> (a,b) and (CuNiFeCoMg)O<sub>x</sub>-Al<sub>2</sub>O<sub>3</sub> (c,d) synthesized using mechanochemical NHSG method.

Subsequently, the catalytic activities of different mesoporous metal oxides are evaluated for CO oxidation (**Figure 3b**). The T<sub>100</sub> values (temperature for 100% CO conversion) are 220 °C (CuO-Al<sub>2</sub>O<sub>3</sub>), 270 °C (Co<sub>3</sub>O<sub>4</sub>-Al<sub>2</sub>O<sub>3</sub>) and 260 °C ((CuNiFeCoMg)O<sub>x</sub>-Al<sub>2</sub>O<sub>3</sub>), respectively. Among these catalysts, Mn<sub>3</sub>O<sub>4</sub>-Al<sub>2</sub>O<sub>3</sub> exhibits much worse activity for the oxidation of CO, which may be attributed to the relatively inactive of Mn<sub>3</sub>O<sub>4</sub> phase. And mesoporous CuO-Al<sub>2</sub>O<sub>3</sub> catalyst become active at 120 °C and CO was completely converted at 220 °C, which are superior to most catalysts especially for Cu-Al mixed oxides prepared

1  
2  
3  
4  
5 using traditional impregnation and precipitation method as shown in Table S2.<sup>[57-59]</sup>  
6  
7  
8 Moreover, both CuO-Al<sub>2</sub>O<sub>3</sub> and (CuNiFeCoMg)O<sub>x</sub>-Al<sub>2</sub>O<sub>3</sub> catalysts exhibited remarkable  
9  
10 stability even after used for 48 h (Figure S16a,b). Considering the facile, fast and solvent-  
11  
12 free preparation method, these mesoporous mixed oxides may have great potential  
13  
14 applications in industrial catalysis. As shown in Figure S17, XRD results of fresh and spent  
15  
16 CuO-Al<sub>2</sub>O<sub>3</sub> and (CuNiFeCoMg)O<sub>x</sub>-Al<sub>2</sub>O<sub>3</sub> catalysts display similar diffraction peaks and  
17  
18 crystallite size. Additionally, temperature programmed desorption (TPD) of CO in Figure  
19  
20 S18 reveals similar CO desorption peak area, indicating the dispersion of metal active species  
21  
22 does not decrease remarkably after use.  
23  
24  
25  
26  
27  
28

29  
30 The sulfur tolerance is of great importance in real-world catalysis. However, CO  
31  
32 oxidation activity of most catalysts went down remarkably in the presence of SO<sub>2</sub>, greatly  
33  
34 affecting the process of industrialization. Therefore, we compared the performance of SO<sub>2</sub>  
35  
36 resistance over CuO-Al<sub>2</sub>O<sub>3</sub> and (CuNiFeCoMg)O<sub>x</sub>-Al<sub>2</sub>O<sub>3</sub> catalysts. Before the catalytic  
37  
38 activity test, each catalyst was treated in 1000 ppm SO<sub>2</sub> at 280 °C for 5 h. The catalytic  
39  
40 activity of CuO-Al<sub>2</sub>O<sub>3</sub> decreased remarkably after SO<sub>2</sub> treatment (Figure S19a). It is  
41  
42 noteworthy that there is a negligible effect of SO<sub>2</sub> on (CuNiFeCoMg)O<sub>x</sub>-Al<sub>2</sub>O<sub>3</sub> catalyst  
43  
44 (Figure S19b). The decreased activity of CuO-Al<sub>2</sub>O<sub>3</sub> is attributed to the formation of sulfites,  
45  
46 evidenced by the feature in FTIR spectra around 1100 cm<sup>-1</sup> (Figure S10).<sup>[60-61]</sup> However, it is  
47  
48 clear that the formation of crystalline high-entropy metal oxides protect itself from SO<sub>2</sub>  
49  
50  
51  
52  
53  
54  
55  
56  
57  
58  
59  
60

1  
2  
3  
4  
5 poisoning, contributing to the superior SO<sub>2</sub> tolerance compared with CuO-Al<sub>2</sub>O<sub>3</sub>. This result  
6  
7 indicates that the (CuNiFeCoMg)O<sub>x</sub>-Al<sub>2</sub>O<sub>3</sub> catalyst may be stabilized by the relative higher  
8  
9 configurational entropy, preventing itself from being sulfurated.<sup>[51]</sup>  
10  
11

## 12 13 **4. Conclusions**

14  
15  
16 In summary, an efficient, fast and facile route for the synthesis of mesoporous Al<sub>2</sub>O<sub>3</sub>  
17  
18 and its metal oxide hybrids has been developed based on mechanochemical non-hydrolytic  
19  
20 method. The obtained meso-Al<sub>2</sub>O<sub>3</sub> shows a record high surface area (~644 m<sup>2</sup> g<sup>-1</sup>) and  
21  
22 uniform pore size (~5 nm). Moreover, mesoporous metal-aluminum oxide and four or five  
23  
24 metal solid solution-aluminum oxide hybrids with rich mesoporous structure and single cubic  
25  
26 crystalline phase was discovered. More importantly, this mechanochemical method does not  
27  
28 need solvents and can shorten the pore filling process from 1 ~ 3 days to 60 min. The obtained  
29  
30 mesoporous mixed metal oxide (such as (CuNiFeCoMg)O<sub>x</sub>-Al<sub>2</sub>O<sub>3</sub>) exhibit not only an  
31  
32 exceptional catalytic performance in CO oxidation, but also the superior SO<sub>2</sub> tolerance. This  
33  
34 mechanochemical NHSG method may open the door to the scalable preparation of a new  
35  
36 class of metal oxide catalysts.  
37  
38  
39  
40  
41  
42  
43  
44  
45  
46  
47

## 48 **Supporting Information**

49  
50  
51 Additional results of characterization results (XRD, SEM, TEM, N<sub>2</sub> adsorption-desorption,  
52  
53  
54 CO-TPD, ICP-AES and FTIR)  
55  
56  
57  
58  
59  
60

## Acknowledgments

S. Dai was supported by the Division of Chemical Sciences, Geosciences, and Biosciences, Office of Basic Energy Sciences, US Department of Energy. J. Fu was supported by the National Natural Science Foundation of China (No. 21436007, 21706228), the Zhejiang Provincial Natural Science Foundation of China (No. LR17B060002). Z. Zhang thanks the China Scholarship Council for financial support as a joint PhD student. P. F. Z. acknowledges Shanghai Pujiang Program (Grant No.17PJ1403500), Thousand Talent Program, National Natural Science Foundation of China (Grant No. 21776174), and the Open Foundation of the State Key Laboratory of Ocean Engineering (Shanghai Jiao Tong University of China) (No. 1809) for the support.

## References

- [1] D. Gu, W. Schmidt, C. M. Pichler, H. J. Bongard, B. Spliethoff, S. Asahina, Z. Cao, O. Terasaki, F. Schüth, Surface-casting synthesis of mesoporous zirconia with a CMK-5-like structure and high surface area. *Angew. Chem. Int. Ed.* **2017**, 56, 11222.
- [2] D. Gu, C.J. Jia, C. Weidenthaler, H.J. Bongard, B. Spliethoff, W. Schmidt, F. Schüth, Highly ordered mesoporous cobalt-containing oxides: structure, catalytic properties, and active sites in oxidation of carbon monoxide. *J. Am. Chem. Soc.* **2015**, 137, 11407.
- [3] Y. Zhou, M. Antonietti, Synthesis of very small TiO<sub>2</sub> nanocrystals in a room-temperature ionic liquid and their self-assembly toward mesoporous spherical aggregates. *J. Am. Chem. Soc.* **2003**, 125, 14960.

- 1  
2  
3  
4  
5 [4] Z. Zhang, F. Zuo, P. Feng, Hard template synthesis of crystalline mesoporous anatase  
6  
7  
8 TiO<sub>2</sub> for photocatalytic hydrogen evolution. *J. Mater. Chem.* **2010**, 20, 2206.  
9
- 10 [5] C. Y. Ma, Z. Mu, J. J. Li, Y. G. Jin, J. Cheng, G. Q. Lu, Z. P. Hao, S. Z. Qiao, Mesoporous  
11  
12  
13 Co<sub>3</sub>O<sub>4</sub> and Au/Co<sub>3</sub>O<sub>4</sub> catalysts for low-temperature oxidation of trace ethylene. *J. Am. Chem.*  
14  
15  
16 *Soc.* **2010**, 132, 2608.  
17
- 18 [6] J. Liu, S. Z. Qiao, Q. H. Hu, G. Q. Lu, Magnetic nanocomposites with mesoporous  
19  
20  
21 structures: synthesis and applications. *Small* **2011**, 7, 425.  
22
- 23 [7] Y. N. Ko, S. B. Park, K. Y. Jung, Y. C. Kang, One-pot facile synthesis of ant-cave-  
24  
25  
26 structured metal oxide-carbon microballs by continuous process for use as anode materials  
27  
28  
29 in Li-ion batteries. *Nano letters* **2013**, 13, 5462.  
30
- 31 [8] Z. Jin, M. Xiao, Z. Bao, P. Wang, J. Wang, A general approach to mesoporous metal oxide  
32  
33  
34 microspheres loaded with noble metal nanoparticles. *Angew. Chem. Int. Ed.* **2012**, 51, 6406.  
35
- 36 [9] W. Xiao, S. Yang, P. Zhang, P. Li, P. Wu, M. Li, N. Chen, K. Jie, C. Huang, N. Zhang, S.  
37  
38  
39 Dai, Facile synthesis of highly porous metal oxides by mechanochemical nanocasting. *Chem.*  
40  
41  
42 *Mater.* **2018**, 30, 2924.  
43
- 44 [10] W.C. Li, A.H. Lu, C. Weidenthaler, F. Schüth, Hard-templating pathway to create  
45  
46  
47 mesoporous magnesium oxide. *Chem. Mater.* **2004**, 16, 5676.  
48
- 49 [11] D. Gu, W. Li, F. Wang, H. Bongard, B. Spliethoff, W. Schmidt, C. Weidenthaler, Y. Xia,  
50  
51  
52  
53  
54 D. Zhao, F. Schüth, Controllable synthesis of mesoporous peapod-like Co<sub>3</sub>O<sub>4</sub>@carbon  
55  
56  
57  
58  
59  
60

1  
2  
3  
4  
5 nanotube arrays for high-performance lithium-ion batteries. *Angew. Chem. Int. Ed.* **2015**, 54,  
6  
7  
8 7060.

9  
10 [12] H. Liu, W. Li, D. Shen, D. Zhao, G. Wang, Graphitic carbon conformal coating of  
11  
12 mesoporous TiO<sub>2</sub> hollow spheres for high-performance lithium ion battery anodes. *J. Am.*  
13  
14  
15  
16  
17  
18  
19  
20  
21  
22  
23  
24  
25  
26  
27  
28  
29  
30  
31  
32  
33  
34  
35  
36  
37  
38  
39  
40  
41  
42  
43  
44  
45  
46  
47  
48  
49  
50  
51  
52  
53  
54  
55  
56  
57  
58  
59  
60  
*Chem. Soc.* **2015**, 137, 13161.

[13] M. Zhen, B. Zhou, Y. Ren, Crystalline mesoporous transition metal oxides: hard-  
templating synthesis and application in environmental catalysis. *Front. Env. Sci. Eng.* **2013**,  
7, 341.

[14] V. Malgras, H. Atae-Esfahani, H. Wang, B. Jiang, C. Li, K. C. W. Wu, J. H. Kim, Y.  
Yamauchi, Nanoarchitectures for mesoporous metals. *Adv. Mater.* **2016**, 28, 993.

[15] W. Li, D. Zhao, An overview of the synthesis of ordered mesoporous materials. *Chem.*  
*Commun.* **2013**, 49, 943.

[16] H. Yang, D. Zhao, Synthesis of replica mesostructures by the nanocasting strategy. *J.*  
*Mater. Chem.* **2005**, 15, 1217.

[17] J. Lee, M. C. Orilall, S. C. Warren, M. Kamperman, F. J. DiSalvo, U. Wiesner, Direct  
access to thermally stable and highly crystalline mesoporous transition-metal oxides with  
uniform pores. *Nat. Mater.* **2008**, 7, 222.

[18] Y. Ren, Z. Ma, P. G. Bruce, Ordered mesoporous metal oxides: synthesis and  
applications. *Chem. Soc. Rev.* **2012**, 41, 4909.

1  
2  
3  
4  
5 [19] W. Yue, W. Zhou, Porous crystals of cubic metal oxides templated by cage-containing  
6  
7 mesoporous silica. *J. Mater. Chem.* **2007**, 17, 4947. 19.

10 [20] X. Sun, Y. Shi, P. Zhang, C. Zheng, X. Zheng, F. Zhang, Y. Zhang, N. Guan, D. Zhao,  
11  
12 G. D. Stucky, Container effect in nanocasting synthesis of mesoporous metal oxides. *J. Am.*  
13  
14  
15  
16  
17  
18  
19  
20  
21  
22  
23  
24  
25  
26  
27  
28  
29  
30  
31  
32  
33  
34  
35  
36  
37  
38  
39  
40  
41  
42  
43  
44  
45  
46  
47  
48  
49  
50  
51  
52  
53  
54  
55  
56  
57  
58  
59  
60  
*Chem. Soc.* **2011**, 133, 14542.

[21] J.-H. Smått, C. Weidenthaler, J. B. Rosenholm, M. Lindén, Hierarchically porous metal  
oxide monoliths prepared by the nanocasting route. *Chem. Mater.* **2006**, 18, 1443.

[22] P. Yang, D. Zhao, D. I. Margolese, B. F. Chmelka, G. D. Stucky, Generalized syntheses  
of large-pore mesoporous metal oxides with semicrystalline frameworks. *Nature* **1998**, 396,  
152.

[23] Z. Zhang, Y. Zhu, H. Asakura, B. Zhang, J. Zhang, M. Zhou, Y. Han, T. Tanaka, A. Wang,  
T. Zhang, Thermally stable single atom Pt/m-Al<sub>2</sub>O<sub>3</sub> for selective hydrogenation and CO  
oxidation. *Nat. Commun.* **2017**, 8, 16100.

[24] Q. Yuan, A.-X. Yin, C. Luo, L.-D. Sun, Y.W. Zhang, W.T. Duan, H.C. Liu, C.H. Yan,  
Facile synthesis for ordered mesoporous  $\gamma$ -aluminas with high thermal stability. *J. Am. Chem.*  
*Soc.* **2008**, 130, 3465.

[25] G. Feng, J. Wang, M. Boronat, Y. Li, J.H. Su, J. Huang, Y. Ma, J. Yu, Radical-facilitated  
green synthesis of highly ordered mesoporous silica materials. *J. Am. Chem. Soc.* **2018**, 140,  
4770.

1  
2  
3  
4  
5 [26] D. M. Antonelli, J. Y. Ying, Synthesis of hexagonally packed mesoporous TiO<sub>2</sub> by a  
6  
7 modified sol-gel method. *Angew. Chem. Int. Ed.* **1995**, 34, 2014.

10 [27] W. Zhou, W. Li, J.-Q. Wang, Y. Qu, Y. Yang, Y. Xie, K. Zhang, L. Wang, H. Fu, D. Zhao,  
11  
12 Ordered mesoporous black TiO<sub>2</sub> as highly efficient hydrogen evolution photocatalyst. *J. Am.*  
13  
14  
15  
16  
17  
18  
19  
20  
21  
22  
23  
24  
25  
26  
27  
28  
29  
30  
31  
32  
33  
34  
35  
36  
37  
38  
39  
40  
41  
42  
43  
44  
45  
46  
47  
48  
49  
50  
51  
52  
53  
54  
55  
56  
57  
58  
59  
60  
*Chem. Soc.* **2014**, 136, 9280.

[28] Y. Zhu, Y. Zhao, J. Ma, X. Cheng, J. Xie, P. Xu, H. Liu, H. Liu, H. Zhang, M. Wu,  
Mesoporous tungsten oxides with crystalline framework for highly sensitive and selective  
detection of foodborne pathogens. *J. Am. Chem. Soc.* **2017**, 139, 10365.

[29] Y. Li, W. Luo, N. Qin, J. Dong, J. Wei, W. Li, S. Feng, J. Chen, J. Xu, A. A. Elzatahry,  
Highly ordered mesoporous tungsten oxides with a large pore size and crystalline framework  
for H<sub>2</sub>S sensing. *Angew. Chem. Int. Ed.* **2014**, 53, 9035.

[30] Y. Wang, C. M. Yang, W. Schmidt, B. Spliethoff, E. Bill, F. Schüth, Weakly  
ferromagnetic ordered mesoporous Co<sub>3</sub>O<sub>4</sub> synthesized by nanocasting from vinyl-  
functionalized cubic *Ia3d* mesoporous silica. *Adv. Mater.* **2005**, 17, 53.

[31] M. Klimakow, P. Klobes, A. F. Thünemann, K. Rademann, F. Emmerling,  
Mechanochemical synthesis of metal-organic frameworks: a fast and facile approach toward  
quantitative yields and high specific surface areas. *Chem. Mater.* **2010**, 22, 5216.

1  
2  
3  
4  
5 [32] A. Savateev, D. Dontsova, B. Kurpil, M. Antonietti, Highly crystalline poly(heptazine  
6 imides) by mechanochemical synthesis for photooxidation of various organic substrates  
7 using an intriguing electron acceptor-Elemental sulfur. *J. Catal.* **2017**, 350, 203.

8  
9  
10  
11  
12  
13 [33] W. Cai, S. Zhang, X. Hu, M. Jaroniec, In situ synthesis of nitrogen-enriched activated  
14 carbons from *procambarus clarkii* shells with enhanced CO<sub>2</sub> adsorption performance. *Energy*  
15 *Fuels* **2018**, 32, 9701.

16  
17  
18  
19  
20  
21 [34] D. Chen, J. Zhao, P. Zhang, S. Dai, Mechanochemical synthesis of metal–organic  
22 frameworks. *Polyhedron* **2019**, 59, 64.

23  
24  
25  
26  
27 [35] J. Zhao, Y. Shu, P. Zhang, Solid-state CTAB-assisted synthesis of mesoporous Fe<sub>3</sub>O<sub>4</sub>  
28 and Au@Fe<sub>3</sub>O<sub>4</sub> by mechanochemistry. *Chinese J. Catal.* **2019**, 40, 1078.

29  
30  
31  
32 [36] Y. Jin, Q. Sun, G. Qi, C. Yang, J. Xu, F. Chen, X. Meng, F. Deng, F. S. Xiao, Solvent-  
33 free synthesis of silicoaluminophosphate zeolites. *Angew. Chem., Int. Ed.* **2013**, 52, 9172.

34  
35  
36  
37 [37] P. Zhang, L. Wang, S. Yang, J. A. Schott, X. Liu, S. M. Mahurin, C. Huang, Y. Zhang, P.  
38 F. Fulvio, M. F. Chisholm, S. Dai, Solid-state synthesis of ordered mesoporous carbon  
39 catalysts via a mechanochemical assembly through coordination cross-linking. *Nat. Commun.*  
40 **2017**, 8, 15020.

41  
42  
43  
44 [38] F. Liu, K. Huang, Q. Wu, S. Dai, Solvent-free self-assembly to the synthesis of nitrogen-  
45 doped ordered mesoporous polymers for highly selective capture and conversion of CO<sub>2</sub>. *Adv.*  
46 *Mater.* **2017**, 29, 1700445.

1  
2  
3  
4  
5 [39] S. M. Morris, P. F. Fulvio, M. Jaroniec, Ordered mesoporous alumina-supported metal  
6  
7  
8 oxides. *J. Am. Chem. Soc.* **2008**, 130, 15210.

9  
10 [40] A. A. Gonçalves, M. J. Costa, L. Zhang, F. Ciesielczyk, M. Jaroniec, One-pot synthesis  
11  
12  
13 of  $\text{MeAl}_2\text{O}_4$  (Me= Ni, Co, or Cu) supported on  $\gamma\text{-Al}_2\text{O}_3$  with ultralarge mesopores: enhancing  
14  
15  
16 interfacial defects in  $\gamma\text{-Al}_2\text{O}_3$  to facilitate the formation of spinel structures at lower  
17  
18  
19 temperatures, *Chem. Mater.* **2018**, 30, 436-446.

20  
21 [41] A. A. Gonçalves, M. Jaroniec, Evaporation-induced self-assembly synthesis of  
22  
23  
24 nanostructured alumina-based mixed metal oxides with tailored porosity, *J. Colloid Interf.*  
25  
26  
27 *Sci.* **2019**, 537, 725-735.

28  
29 [42] A. A. Gonçalves, P. B. Faustino, J. M. Assaf, M. Jaroniec, One-pot synthesis of  
30  
31  
32 mesoporous Ni–Ti–Al ternary oxides: highly active and selective catalysts for steam  
33  
34  
35 reforming of ethanol, *ACS Appl. Mater. Interf.* **2017**, 9, 6079-6092.

36  
37 [43] W. Cai, J. Yu, C. Anand, A. Vinu, M. Jaroniec, Facile synthesis of ordered mesoporous  
38  
39  
40 alumina and alumina-supported metal oxides with tailored adsorption and framework  
41  
42  
43 properties, *Chem. Mater.* **2011**, 23, 1147-1157.

44  
45 [44] B. Tian, X. Liu, B. Tu, C. Yu, J. Fan, L. Wang, S. Xie, G. D. Stucky, D. Zhao, Self-  
46  
47  
48 adjusted synthesis of ordered stable mesoporous minerals by acid-base pairs. *Nat. Mater.*  
49  
50  
51 **2003**, 2, 159.

- 1  
2  
3  
4  
5 [45] D. P. Debecker, K. Bouchmella, C. Poleunis, P. Eloy, P. Bertrand, E. M. Gaigneaux, P.  
6  
7 H. Mutin, Design of SiO<sub>2</sub>–Al<sub>2</sub>O<sub>3</sub>–MoO<sub>3</sub> metathesis catalysts by nonhydrolytic sol-gel. *Chem.*  
8  
9 *Mater.* **2009**, 21, 2817.
- 10  
11  
12  
13 [46] Y. Liu, M. Wang, Z. Li, H. Liu, P. He, J. Li, Preparation of porous  
14  
15 aminopropylsilsesquioxane by a nonhydrolytic sol-gel method in ionic liquid solvent.  
16  
17 *Langmuir* **2005**, 21, 1618.
- 18  
19  
20  
21 [47] H. Liu, Y. Li, C. Yin, Y. Wu, Y. Chai, D. Dong, X. Li, C. Liu, One-pot synthesis of  
22  
23 ordered mesoporous NiMo–Al<sub>2</sub>O<sub>3</sub> catalysts for dibenzothiophene hydrodesulfurization. *Appl.*  
24  
25 *Catal. B: Environ.* **2016**, 198, 493.
- 26  
27  
28  
29 [48] D. P. Debecker, V. Hulea, P. H. Mutin, Mesoporous mixed oxide catalysts via non-  
30  
31 hydrolytic sol-gel: a review. *Appl. Catal. A*: **2013**, 451, 192.
- 32  
33  
34  
35 [49] J. L. Gunjakar, T. W. Kim, H. N. Kim, I. Y. Kim, S.J. Hwang, Mesoporous layer-by-  
36  
37 layer ordered nanohybrids of layered double hydroxide and layered metal oxide: highly  
38  
39 active visible light photocatalysts with improved chemical stability. *J. Am. Chem. Soc.* **2011**,  
40  
41  
42  
43 133, 14998.
- 44  
45  
46 [50] H. Jiang, H. Bongard, W. Schmidt, F. Schüth, One-pot synthesis of mesoporous Cu–γ-  
47  
48 Al<sub>2</sub>O<sub>3</sub> as bifunctional catalyst for direct dimethyl ether synthesis. *Microp. Mesopo. Mater.*  
49  
50  
51 **2012**, 164, 3.
- 52  
53  
54  
55  
56  
57  
58  
59  
60

- 1  
2  
3  
4  
5 [51] C. M. Rost, E. Sachet, T. Borman, A. Moballegh, E. C. Dickey, D. Hou, J.L. Jones, S.  
6  
7  
8 Curtarolo, J.P. Maria, Entropy-stabilized oxides. *Nat. Commun.* **2015**, 6, 8485.  
9
- 10 [52] A. Sarkar, L. Velasco, D. Wang, Q. Wang, G. Talasila, L. de Biasi, C. Kubel, T.  
11  
12 Brezesinski, S. S. Bhattacharya, H. Hahn, B. Breitung, High entropy oxides for reversible  
13  
14 energy storage. *Nat. Commun.* **2018**, 9, 3400.  
15  
16  
17  
18 [53] H. Chen, J. Fu, P. Zhang, H. Peng, C. W. Abney, K. Jie, X. Liu, M. Chi, S. Dai, Entropy-  
19  
20 stabilized metal oxide solid solutions as CO oxidation catalysts with high-temperature  
21  
22 stability. *J. Mater. Chem. A* **2018**, 6, 11129.  
23  
24  
25  
26 [54] A. Sarkar, R. Djenadic, N. J. Usharani, K. P. Sanghvi, V. S. Chakravadhanula, A. S.  
27  
28 Gandhi, H. Hahn, S. S. Bhattacharya, Nanocrystalline multicomponent entropy stabilised  
29  
30 transition metal oxides. *J. Eur. Ceram. Soc.* **2017**, 37, 747.  
31  
32  
33  
34 [55] Z. Zhang, Q. Yang, H. Chen, K. Chen, X. Lu, P. Ouyang, J. Fu, JG. Chen, In situ  
35  
36 hydrogenation and decarboxylation of oleic acid into heptadecane over a Cu–Ni alloy catalyst  
37  
38 using methanol as a hydrogen carrier. *Green Chem.* **2018**, 20(1):197  
39  
40  
41  
42 [56] L. Óvári, S.K. Calderon, Y. Lykhach, J. Libuda, A. Erdőhelyi, C. Papp, J. Kiss, H.P.  
43  
44 Steinrück, Near ambient pressure XPS investigation of the interaction of ethanol with  
45  
46 Co/CeO<sub>2</sub> (111). *J. Catal.* **2013**, 307, 132.  
47  
48  
49  
50  
51  
52  
53  
54  
55  
56  
57  
58  
59  
60

- 1  
2  
3  
4  
5 [57] S. Nikolaev, E. Golubina, I. Krotova, M. Shilina, A. Chistyakov, V. Kriventsov, The  
6  
7 effect of metal deposition order on the synergistic activity of Au-Cu and Au-Ce metal oxide  
8  
9 catalysts for CO oxidation. *Appl. Catal. B: Environ.* **2015**, 168, 303.  
10  
11  
12 [58] M.F. Luo, P. Fang, M. He, Y.L. Xie, In situ XRD, Raman, and TPR studies of CuO/Al<sub>2</sub>O<sub>3</sub>  
13  
14 catalysts for CO oxidation. *J. Mol. Catal. A: Chem.* **2005**, 239, 243.  
15  
16  
17 [59] G. Pantaleo, L. Liotta, A. Venezia, G. Deganello, E. Ezzo, M. El Kherbawi, H. Atia,  
18  
19 Support effect on the structure and CO oxidation activity of Cu-Cr mixed oxides over Al<sub>2</sub>O<sub>3</sub>  
20  
21 and SiO<sub>2</sub>. *Mater. Chem. Phys.* **2009**, 114, 604.  
22  
23  
24 [60] A. Goodman, P. Li, C. Usher, V. Grassian, Heterogeneous uptake of sulfur dioxide on  
25  
26 aluminum and magnesium oxide particles. *J. Phys. Chem: A* **2001**, 105, 6109.  
27  
28  
29 [61] F. F.Chen, K. Huang K, J. P. Fan, D. J. Tao D, Chemical solvent in chemical solvent: a  
30  
31 class of hybrid materials for effective capture of CO<sub>2</sub>, *AIChE J.* **2018**, 64, 632.  
32  
33  
34  
35  
36  
37  
38  
39  
40  
41  
42  
43  
44  
45  
46  
47  
48  
49  
50  
51  
52  
53  
54  
55  
56  
57  
58  
59  
60

## Table of Contents

The facile, solvent-free and scalable preparation of mesoporous metal oxides and metal oxide hybrids is complete by a mechanochemical nonhydrolytic sol-gel approach. The obtained meso- $\text{Al}_2\text{O}_3$  shows a record high surface area ( $\sim 644 \text{ m}^2 \text{ g}^{-1}$ ) and uniform pore size ( $\sim 5 \text{ nm}$ ). More importantly, four or five metal species-aluminum oxide hybrids—the so-called high-entropy oxide—with rich mesoporous structure and single cubic crystalline phase are also discovered. The obtained  $(\text{CuNiFeCoMg})\text{O}_x\text{-Al}_2\text{O}_3$  sample exhibits surprising  $\text{SO}_2$  resistance than  $\text{CuO-Al}_2\text{O}_3$  owing to the formation of more stable high-entropy phase.

